Interaction Region Layout, Feedback and Background Issues for TESLA

O. Napoly
CEA/Saclay, DAPNIA-SEA, 91191 Gif-sur-Yvette, France

I. Reyzl, N. Tesch
Deutsches Elektronen-Synchrotron, Notkestrasse 85, 22603 Hamburg, Germany

We present the current design of the interaction region for the superconducting linear collider project TESLA. We describe the layout of magnets, separators and collimators which are needed to accommodate a small vertex detector radius in the large aperture appropriate for the head-on collision scheme of TESLA. We then describe the feedback system which will be used to vertically stabilize the beam collisions on a bunch-to-bunch basis down to a fraction of the beam spot size of 5nm. We finally review the various background levels in the detector region, with special attention to the impact of e^+e^- pair and secondary neutron production on the design of the TESLA detector.

1 Introduction

The TESLA superconducting linear collider project [1] aims to produce e^+e^- collisions at 500GeV c.m. energy with luminosity in excess of $10^{34}\mathrm{cm}^{-2}\mathrm{s}^{-1}$. The current parameters of the collider[2] are given in table 1. The design of its interaction region (IR) is mostly driven by three basic ingredients:

- The optics of beam focusing and extraction around the interaction point (IP)
- The diagnostics and correction systems required for reaching and maintaining stable beam operation at the nominal luminosity
- The shielding of nearby components and the masking of the experiment detector from the various accelerator and beam-beam induced background flux

The TESLA final focus optics has some similarities with that of the SLC collider: the beams are focused by high gradient superconducting low-beta quadrupoles with large aperture and they collide at zero crossing angle and are extracted outside of the detector. Indeed, taking advantage of the long RF pulse allowed by the TESLA superconducting linear accelerators, the successive bunches of the TESLA bunch train are equally spaced by about 340ns. It is therefore possible to extract the outgoing beam with a long electrostatic and magnetic separator well before the first parasitic crossing point at about 50m from the IP. However, unlike the SLC, the final doublet quadrupoles are the only magnets common to the incoming and outgoing beam lines. The tuning of both beam lines is therefore coupled in a minimum way.

The luminosity optimization relies on reaching and stabilizing maximum beam overlap and nominal beam sizes at the IP. After the initial tuning of both beam optics separately, this optimization can be divided into three successive levels of tuning procedures:

- The position and angle differences of the colliding bunches at the IP must be cancelled. Thanks to the TESLA pulse structure, the beam separation

can be corrected within a small fraction of the bunch train by a dedicated IP feedback system, as discussed in section 3. This procedure must be repeated on a pulse to pulse basis.

- The transverse beam sizes and linear beam moments (waist-motion, coupling, dispersion, etc..) are measured and tuned. The measurement of the linear beam matrix can be done with a few pulses, using horizontal beam-beam scans for the purely horizontal moments, and luminosity monitoring for the vertical moments and coupling. The correction will be performed by upstream corrector magnets and is believed to remain stable long enough compared to the 5Hz pulse frequency with a slow feedback system steering the beam to a reference orbit.
- Even though the linear optics will be periodically re-tuned, higher order aberrations will slowly develope due to the slow motion of the final focus magnets. The induced degradation of the collider luminosity can be corrected only by beam based re-alignment of the most sensitive elements, like the sextupoles.

Finally, the detector masking and magnet shielding must integrate two specific features of the TESLA design:

- Due to the zero crossing angle, the photon background irradiates the incoming beam line. It is composed of a) high energy beamstrahlung photons, 12GeV energy in average, carrying 300kW average power per side which can damage magnets, and b) widespread synchrotron radiation, 8MeV and 2.1kW average power, produced mostly by the spent beam through the outgoing doublet, which can scatter on close-by elements back to the detector.
- In the current design, the e^- beam must be extracted and transported to the positron target with small beam loss. To accommodate for the capture beam line, the spent beam is bent in the horizontal plane with septum magnets providing the final deflection.

Table 1: Main parameters of the TESLA linear collider.

Parameter	Symbol	Unit	Reference Design
Center of mass energy	E_{cm}	GeV	500
Repetition rate	f_{rep}	Hz	5
Bunch No. per pulse	n_b		2820
Pulse length	t_{pulse}	μs	950
Bunch spacing	t_{bunch}	ns	337
Bunch charge	N	1/e	$2 \cdot 10^{10}$
Horizontal rms beam size at IP	$\sigma_x^\star$	nm	553
Vertical rms beam size at IP	$\sigma_y^\star$	nm	5
Vertical divergence at IP	$\sigma_{y'}^\star$	μrad	12.3
Vertical Disruption	D_y		33
Luminosity	L_0	$\mathrm{cm}^{-2}\mathrm{s}^{-1}$	$3.1 \cdot 10^{34}$

2 TESLA: Interaction Region Layout

The optics of the beam focusing to the interaction point, depicted in figure 1, is mostly determined by the choice of the free space distance, $l^* = 3$m, from the last

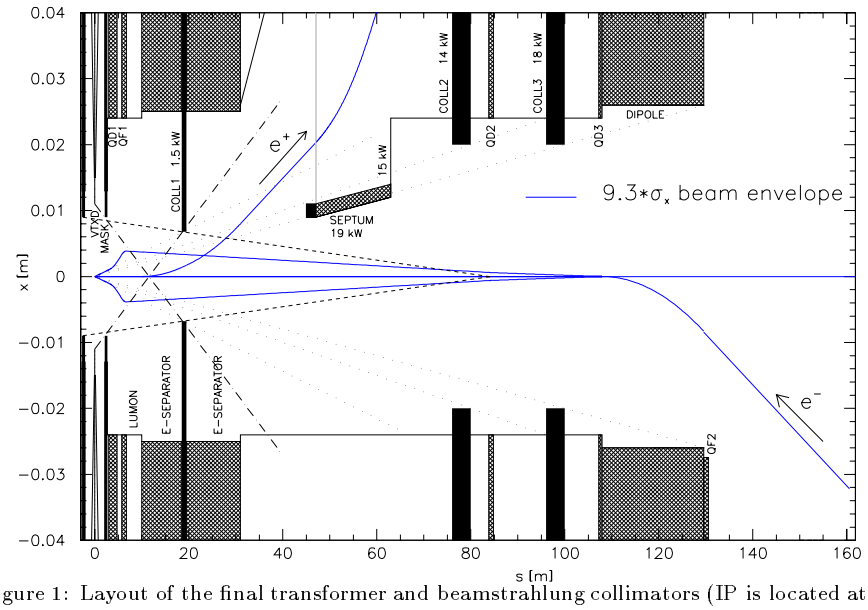

Figure 1: Layout of the final transformer and beamstrahlung collimators (IP is located at s=0).

quadrupole exit to the IP, together with that of the quadrupole magnet superconducting technology. Such quadrupoles[3], combined in a doublet (QF1,QD1), provide the required focusing strength, $G = 250\text{T/m}$, with a large aperture, $R = 24\text{mm}$, necessary to extract the beam as well as the synchrotron radiation background. Their cross section is shown in figure 2(a). These iron-free quadrupoles can stand up to 3T solenoid field with usual NbTi conductors, and over 4T with Nb_3Sn cables. A Tungsten mask with a cylindrical part around the quadrupole cryostat and a 83mrad conical part, as shown in figure 2(b), has been designed [4] to stop the e^+e^- pairs created during the beam-beam interaction and to protect the detector from secondary photons. It also includes an inner cylindrical part to stop the pairs backscattered from the quadrupole face, and to damp the flux of neutrons produced in the collimators outside from the detector. These neutrons are particularly harmful for the vertex detector. Therefore the aperture radius of the inner mask is matched to the radius of the beam pipe at the vertex detector. In figure 2(b), a radius of 18mm was assumed for a 20mm beam pipe radius. In the following study, the mask aperture is reduced to 9mm radius to be able to accommodate a more ambitious design of the vertex detector around a beam pipe radius of 11mm. The role and the performance of the mask will be discussed in more details in section 4.

After the interaction point, the outgoing beam undergoes a first deflection of 8mrad over 20m from an electrostatic separator with $E_x = 48\text{kV/cm}$ across a 5cm gap, combined with a dipole magnet with $B_y = 0.016\text{T}$ in such way that the force acting on the incoming beam, and its polarization, is cancelled. Later, an array of septum magnets over 16m length, provides a second deflection of 2.1mrad to bring

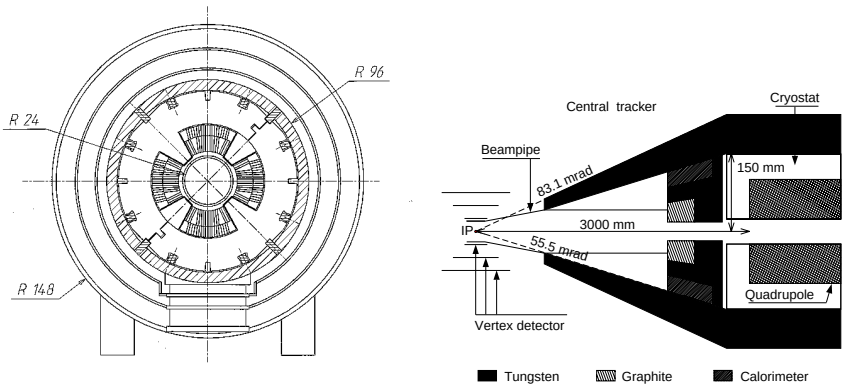

Figure 2: Low-beta SC quadrupole cross section (a) and detector masking system (b).

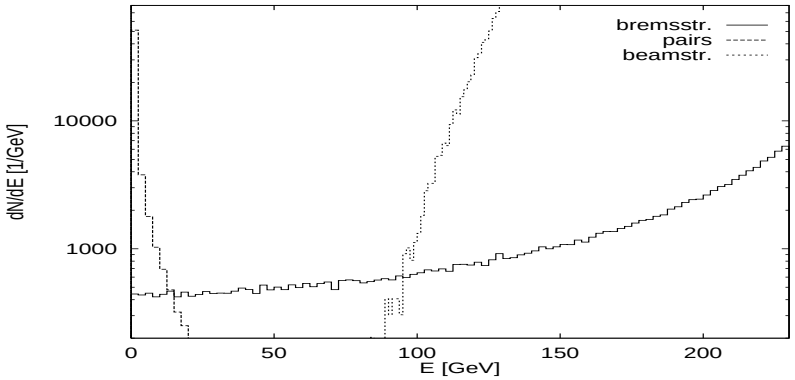

Figure 3: Spectrum of charged particles leaving the IP for a nominal head-on collision.

the spent beam to its capture beam line towards the positron target.

The collimation of the 300kW beamstrahlung photon flux, with about $150 \cdot 34\,\mu\text{rad}^2$ rms divergence from the IP, is done by staged collimators. Figure 1 shows the location of the first four collimators and indicates the amount of beamstrahlung power which they intercept. Collimators 2 and 3 , with a radius of 20mm, are positioned to protect the downstream magnets including the first dipole. The septum is protected by a 2mm thin collimator directly in front of it. The primary role of collimator 1 is to shield the inner part the detector, including the two symmetric inner masks, from the incoming synchrotron radiation generated by the dipole and the quadrupoles up to QD2. Its location is optimized by requiring that, by being close to the IP, its aperture defined by the dashed line of sight from QD2 in figure 1 is large and therefore intercepts as little beamstrahlung power as possible while, by being sufficiently away from the IP, no synchrotron radiation photon can scatter from its edge directly to the beam pipe at the IP, as shown by the dashed-dotted line of sight in figure 1. The optimum location is roughly 19m from the IP. Collimator 1, with an aperture radius of 7mm, thus splits the electrostatic separator in two parts.

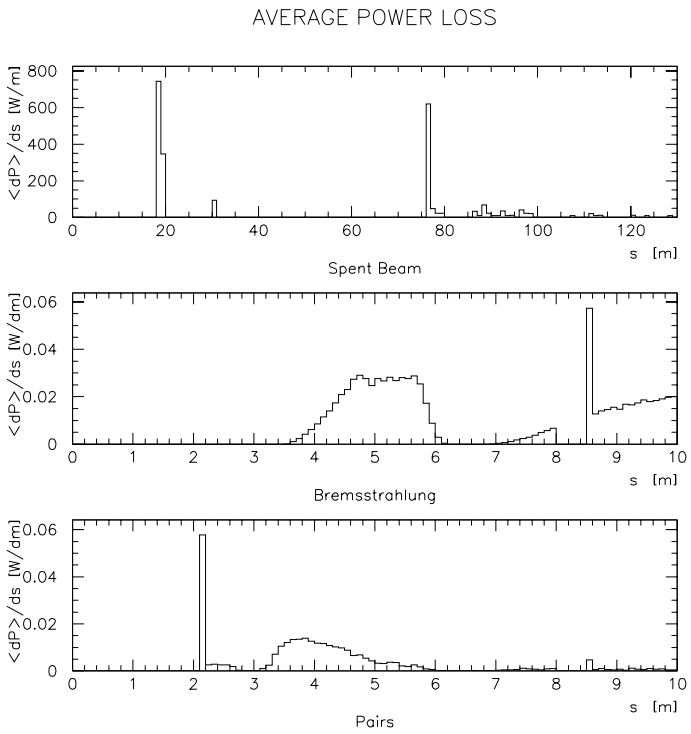

Figure 4: Average power loss along the opposing beam line (the septum collimator is not included in the calculation of the spent beam losses).

This is advantageous because it also intercepts about 1.1kW of spent beam power, as discussed in the next paragraph, and a large fraction of the 2.1kW synchrotron radiation power emitted in the outgoing doublet which would otherwise hit the electrodes of the separator and possibly induce sparking. Except for the quadrupole QF2, figure 1 does not show the location and aperture of the magnets which are centered along the incoming beam line upstream of the dipole. These elements can be shielded from the remaining 240kW of beamstrahlung either by dumping the beamstrahlung flux about 20m after the dipole or, by using flat beam chambers which extend horizontally through the poles of the magnets towards and beyond the beamstrahlung axis in order to clear the photons. In this case the remaining beamstrahlung power can be dumped further down.

To quantify the steady beam losses along the outgoing beam line, we use the distribution of the charged particles after the collision point, assuming ideal beam collisions, obtained from GUINEA_PIG beam-beam simulations[5]. The charged particle spectrum, shown in figure 3, is the superposition of the energy degraded spent beam, at high energy, of the e^+e^- pairs at low energy and, the radiative Bhabha (or *bremsstrahlung*) particles which dominate between roughly 20 and 100GeV. The average deposited power per unit length is shown in figure 4. The pair and radiative Bhabha losses are plotted only along the first 10m after the IP since the spent beam

completely dominates the power loss beyond this point. It is important to note that the power levels along the superconducting doublet cryostat, from 3 to 6.5m, are well below the 4.7W/m LHC tolerance [6]. The spikes in the spent beam power loss correspond to the location of collimators 1 and 2, but the collimator in front of the septum magnet has not been included in the calculation. The spike in the pair power loss is of course at the inner mask face. Finally, the spike in the radiative Bhabha power corresponds to the location of the fast luminosity monitor [7]. It is produced by introducing a gap in the beam pipe from 8 to 8.5m after the IP in order to collect the radiative Bhabhas. Figure 4 shows that higher statistics and less secondary background could be obtained by opening the beam pipe already at 7m from the IP.

3 Feedback System at IP

Due to the large vertical disruption parameter D_y=33, the luminosity is very sensitive to beam separations and crossing angles in the vertical plane, see figure 5. Limiting the maximum luminosity loss per bunch crossing to 10%, two bunches have to interact within a separation of $5\text{Å} = 0.1\,\sigma_y^\star$ and with a crossing angle smaller than 1.2μrad.

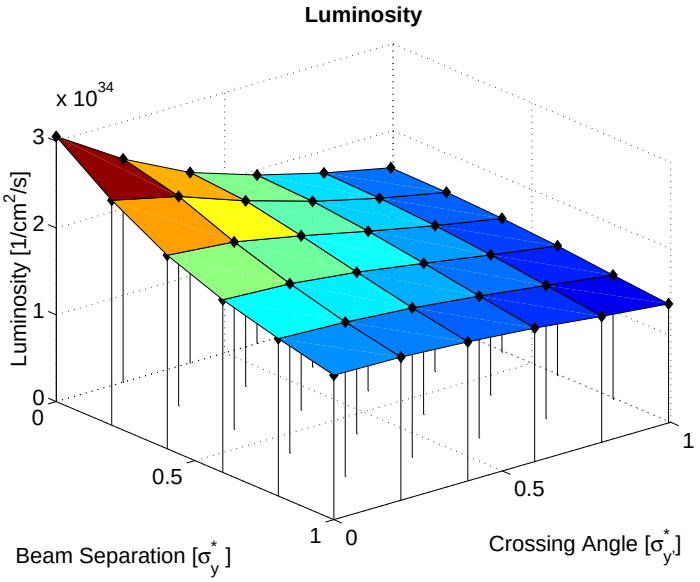

Figure 5: Luminosity as a function of beam separation and crossing angle.

Sources of undesired beam separations and crossing angles are e.g. Lorentz force detuning, wakefield effects and quadrupole vibrations. The displacement of the two opposing final doublet magnets is a major concern, since a stationary final doublet displacement of $5\text{nm} = 1\,\sigma_y^\star$ will half the luminosity. Simulations assuming large contributions of human produced noise to the ground motion spectrum [1] predict a $1\,\sigma_y^\star$ beam separation within 1ms, which is roughly the bunch train length. From

pulse to pulse the expected separation might add up to $20\,\sigma_y^\star$ solely due to ground motion effects in the BDS [8].

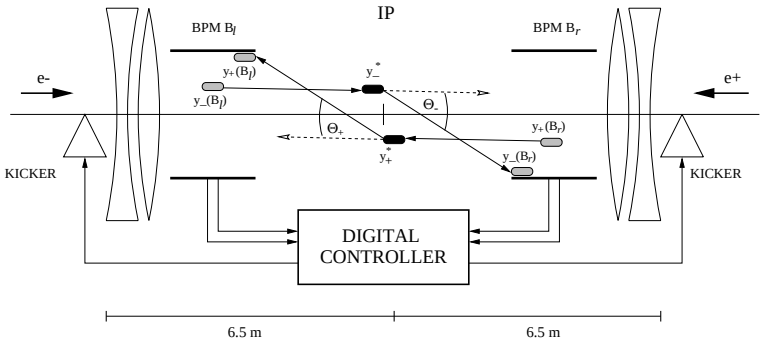

Figure 6: Scheme of the digital feedback system at the IP.

The size and the time scale of the vertical beam separation emphasize the necessity of a feedback system providing a stabilization of the beam interaction at the IP within the bunch train. Due to the large bunch spacing of 337ns a very beneficial correction from one bunch to the second bunch becomes feasible. The design goal is a correction limiting the maximum luminosity loss to 10%. In order to control the other beam angle a further feedback system will remove bunch offsets in the BDS within the bunch train [9].

3.1 IP Feedback Loop

The feedback system at the IP is schematically shown in figure 6. The loop of the digital feedback system (sample frequency 3MHz) is characterized by four steps: detection of bunch separation, estimation of bunch separation, determination of correction kick by a proportional-integral (PI) controller and correction of subsequent bunches by using two fast kickers. The kickers [10], placed on both sides of the IP one meter upstream of the final doublet, allow the coverage of a control range of $\pm 100\,\sigma_y^\star$. The overall processing time of the feedback loop and the signal transmission time in a 50m long cable insert a correction delay of two sample periods. Bunch separations at the IP become detectable by the beam-beam deflection caused by the attraction of the opposite charged bunches [11]. The experienced kick results in measurable position shifts of the outgoing bunches. From the position measurements of the incoming and outgoing bunch of both beams at the two opposing final doublets the size and the sign of the bunch separation can be ascertained.

The separation $\triangle y^\star$ between two bunches is estimated by using a linear model θ^{FB} of the the beam-beam kick, both plotted in figure 7:

$$\theta^{FB}(\triangle y^\star) = -37.27\,\frac{\triangle y^\star}{\sigma_y^\star} \quad [\mu\mathrm{rad}]. \tag{1}$$

The slope of this linear approximation defines how accurately the controller will determine a bunch separation in the nanometer range and by how much large separations will be underestimated.

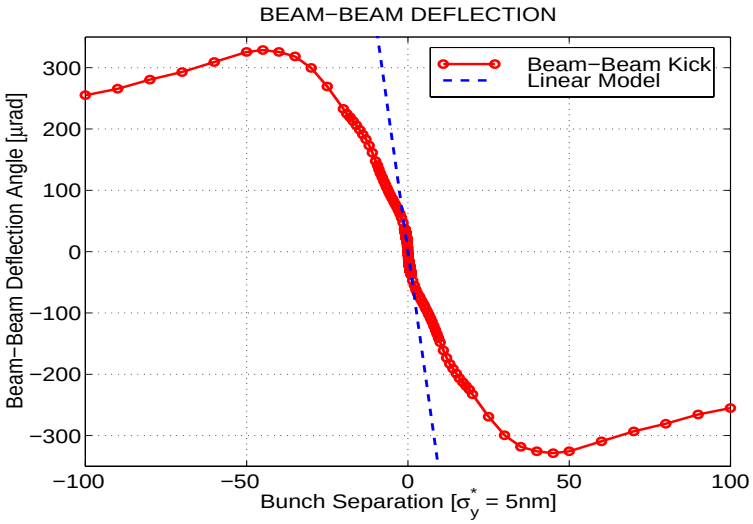

Figure 7: Beam-beam deflection angle θ vs. bunch separation.

3.2 Results

Even though the linear model θ^{FB} used by the feedback system deviates severely from the non-linear beam-beam kick for large separations large stationary offsets are successfully rejected. A constant beam separation of 100 $\sigma_y^\star$ is reduced by 3 orders of magnitude after 80 bunch interactions, emphasizing the robustness of the feedback system to model errors, see figure 8.

During correction the actual vertical separation is continuously underestimated (e.g. $\triangle y^\star = 100\,\sigma_y^\star$ is interpreted as a $7\,\sigma_y^\star$ separation). However, the feedback loop steers subsequent bunches in the right direction decreasing stepwise the occurring offset.

More realistic simulations include the bunch offsets at the linac exit caused by cavity and quadrupole misalignments of 500μm and BPM displacements of 100μm rms. At the IP we further assume a BPM resolution of 5μm (add. noise), quantization errors caused by ADC, a 10% jitter of the beam-beam deflection angle due to bunch charge jitter (mult. noise) and kicker errors of 0.1% (mult. noise). Without the use of a feedback system the luminosity is lowered by 8.4%, whereas a stabilization of the beam interaction by a feedback system allows to achieve 98.6% of the nominal luminosity denoted by L_0.

Assuming an additional stationary beam separation of $50\,\sigma_y^\star$ and $100\,\sigma_y^\star$ caused by ground motion in the BDS and by the displacement of the two final doublets, a luminosity of 95.6% L_0 and 91.8% L_0, respectively, becomes feasible. Limiting the maximum luminosity loss to 10%, the use of the IP feedback system thus relaxes the rms displacement tolerance of pulse-to-pulse jitter of the final doublet magnets to 200nm.

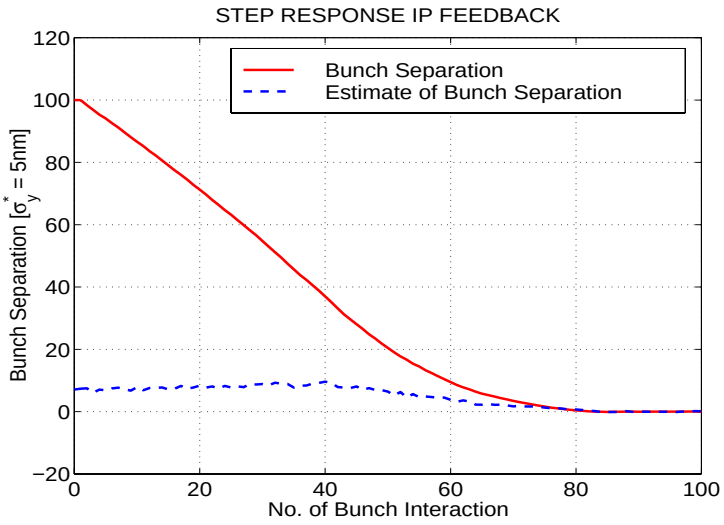

Figure 8: Response to a stationary $100\,\sigma_y^\star$ beam separation.

4 Beam-Beam and Machine Background

4.1 Introduction

The high charge density of the colliding beams produces strong electro-magnetic fields which bend the trajectories of the particles of the oncoming bunch. This focusing effect reduces the effective beam size and enhances the total luminosity. However, at these high energies, this beam-beam interaction also induces an intense emission of hard beamstrahlung photons (in the order of 10^{11} per bunch crossing (BX)) which degrades the energy distribution of the beams during collision. These beamstrahlung photons do not give any direct background signals in the detector, but they can produce a lot of secondary effects, such as pair, charged hadron and neutron production (see figure 9). Beside these beamstrahlung photons, photons can also be created from the elementary process $e^+e^- \rightarrow e^+e^-\gamma$. These photons are no problem as background in the detector, but the remaining electron/positron (radiative Bhabha) whose energy is reduced by the amount of the photon energy can contribute to the neutron background.

On the other hand there are machine related background sources: Muons can be created in electro-magnetic beam-nucleon interactions in the beam delivery system. These muons can reach the IP and can cause an intolerable background in the detector. The collimation system of TESLA is done such that no direct synchrotron radiation can reach the detector. But the edge- and backscattering of the synchrotron radiation of the incoming and outgoing beam from elements of the collimation system can be a potential source of background. Finally beam-gas interactions can contribute to the background in the detector. All background sources are described in more detail elsewhere [1,4].

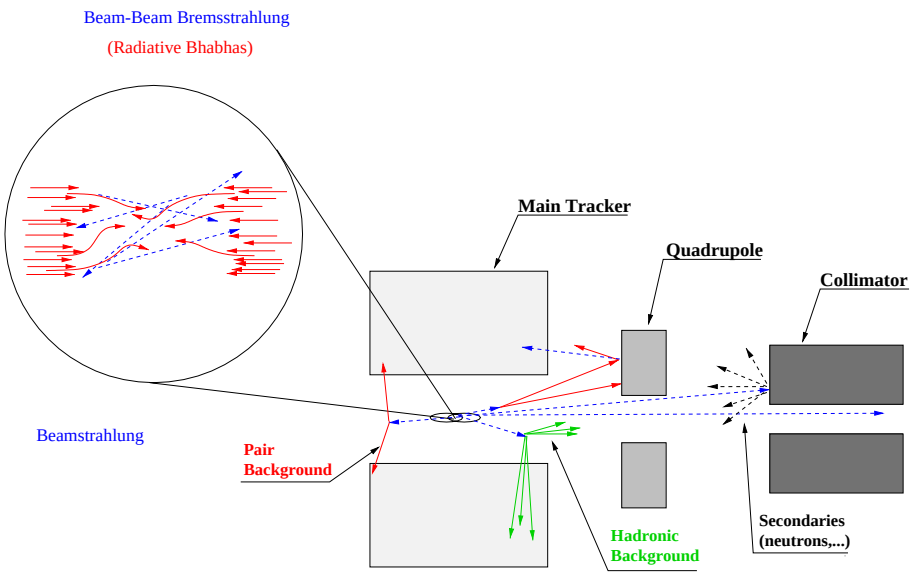

Figure 9: Illustration of different background sources.

4.2 Beamstrahlung

The two bunches focus each other at the interaction point due to the high charge density of beams which leads to strong electro-magnetic fields. This effect is called the 'pinch effect'. Since the particle trajectories are bent due to the pinch effect they emit a radiation called beamstrahlung (BS). This leads to an energy loss of the electrons and positrons. For TESLA the photons have energies in the range of a few GeV. The center of mass energy for the collisions will hence vary more than expected from the energy spread of the incoming beams and the initial state radiation. Since the pinch effect reduces the effective beam cross sections the luminosity is enhanced compared to the nominal one. To study the BS different Monte Carlo programs were developed to simulate the pinch effect and the secondary physical processes. Three generators (GUINEA_PIG [4], CAIN 2.1b [12], LINCOL 1.0 [13]) were used and their results are compared in table 2.

The beamstrahlung photons produced by the program GUINEA_PIG were used as an input to a GEANT3 [14] based simulation of the TESLA detector and beam line called BRAHMS [15]. There were no direct hits from BS in any detector element with the present collimation system found.

4.3 Pairs

One of the main background sources in the detector is the production of electron-positron pairs via coherent or incoherent processes in the beam-beam interaction. The coherent ones can be neglected in the TESLA case. Three main processes contribute to the incoherent production of electron-positron pairs:

Table 2: Comparison of beamstrahlung results from different generators.

	GUINEA_PIG	CAIN 2.1b	LINCOL 1.0
δE_{beam} [GeV]	6.92	6.80	7.62
δE_{beam} [%]	2.77	2.72	3.05
N_γ per electron	1.65	1.62	1.70
$\overline{E_\gamma}$ [GeV]	4.19	4.20	4.48
N_γ / BX [10^{10}]	6.60	6.48	6.80
E_γ / BX [J]	44.3	43.5	48.8
P_γ [MW]	0.63	0.61	0.69

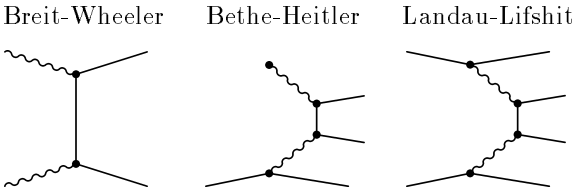

The Bethe-Heitler and Landau-Lifshitz processes can be calculated using the equivalent photon approximation, in which the electron (and positron) are replaced by a spectrum of photons. For the Breit-Wheeler process the two colliding photons are real, where for the Bethe-Heitler one photon is real and one virtual and for the Landau-Lifshitz processes both photons are virtual.

Table 3: Comparison of pair production results from different generators.

	GUINEA_PIG	CAIN 2.1b	LINCOL 1.0
N_{pairs} / BX [10^3]	120	82	73
E_{pairs} / BX [10^3GeV]	295	193	175
$p_t > 20$MeV			
$\theta > 150$mrad			
N_{pairs} / BX	50	32	46
E_{pairs} / BX [GeV]	6.61	3.60	5.95

Again the above described three Monte Carlo programs were used and their results for pair production are compared in table 3. The pair particles produced by the GUINEA_PIG program were tracked through the TESLA detector simulation BRAHMS (see figure 10) and the following results were found: For a radius between 0.9cm and 5.4cm at the front side of the mask the deposited energy is 27.3TeV per BX (26.4TeV per BX) for a main magnetic field of 3T (4T). For radii greater than 5.4cm (corresponding to an angle larger than 23.5mrad) the energy deposition is 6GeV per BX for 3T and 4T. Therefore instrumentation of the front side of the mask seems to be possible for at least angles down to 23.5mrad to measure physics

based events. In the vertex detector of the current design of the TESLA detector there were 690 charged hits per BX in the first layer (at 1.2cm) found for the 3T case and 334 for the 4T case. The number of photons created from pair particles entering the TPC was found to be 1350 per BX (3T) with an average energy of 1.7MeV and 1200 per BX (4T) with an average energy of 1.6MeV. The conclusion can be made that the numbers of photons from the pair background in the TPC is non-critical and that both discussed vertex detector pixel designs (APS,CCD) even for a 1cm beam pipe and 3T main magnetic field are feasible.

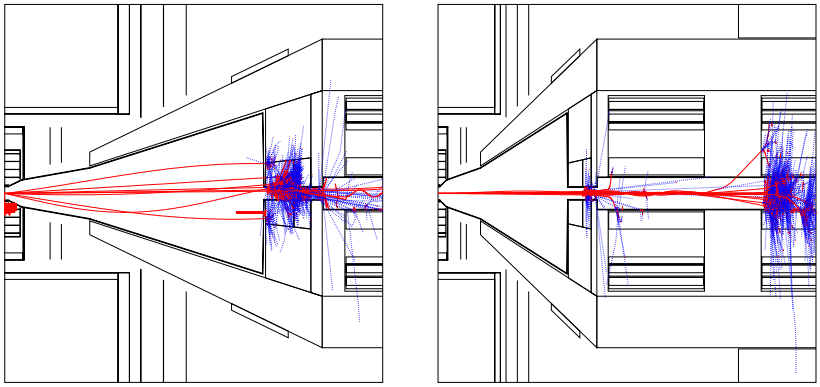

Figure 10: Some pair particles showering at the front side of the mask and some radiative Bhabhas showering at the final quadrupole doublet (from TESLA detector simulation BRAHMS).

4.4 Radiative Bhabhas

Another process that produces low energy particles is the elementary process $e^+e^- \rightarrow e^+e^-\gamma$. Here the beam particle emits a hard photon in the field of a single oncoming particle (beam-beam bremsstrahlung). The calculation is done using the equivalent photon approximation. The photon escapes through the beam pipe, while the remnant beam particle contributes to the background. These low energy beam electrons/positrons, called radiative Bhabhas (RB), will be dumped in the final quadrupole doublet and will produce electro-magnetic showers and neutrons in the material of the quadrupoles (see figure 10). The consequences are that some of the electro-magnetic shower particles (photons/electrons) as well as the produced neutrons from inside the quadrupoles can reach the detector.

As a generator the GUINEA_PIG program was used. Applying a cut of 100GeV (to select only these particles which will hit the final quadrupole doublet) gives a total number of radiative Bhabhas of $N_{tot} = 4.9 \cdot 10^4$ per BX with a total energy of $E_{tot} = 2.6 \cdot 10^6$GeV per BX.

Again these particles were tracked through the TESLA detector simulation with the result that all electrons/positrons with an energy E >90GeV pass the final quadrupole doublet. In the first layer of the vertex detector (at 1.2cm) 2 charged hits per BX were found for a main magnetic field of 3T and the number of photons entering the TPC was found to be 3 per BX for 3T. In conclusion the amount of direct background hits in the detector from radiative Bhabhas is small.

4.5 Neutrons

Neutrons are produced via photo-nuclear reactions from electro-magnetic shower bremsstrahlung photons. The dominant neutron production via the giant photo-nuclear resonance mechanism is in the photon energy range between 10-30MeV. Therefore any γ,e^+,e^- hitting a beam line element and creating electro-magnetic showers is a potential source of neutrons.

The simulation of neutron production was done using the program FLUKA98[16]. This program can handle the production and transport of neutrons from thermal energies up to 20TeV for primary and secondary particles. It can simulate the low energy neutron production down to 0.4eV in ENEA multigroups. The low energy neutron transport is done via photon and fission neutron generation and the photo and electro-hadron/nuclear production is using the vector meson dominance model. The geometry of the TESLA detector and beam line in FLUKA98 can be seen in figure 11.

The total number of neutrons produced from beamstrahlung photons is $N_{tot} = 2.5 \cdot 10^{10}$ per BX with a total energy $E_{tot} = 2.4 \cdot 10^8$GeV per BX. For the pairs these numbers are $N_{tot} = 4.9 \cdot 10^4$ per BX with $E_{tot} = 262$GeV per BX and for the radiative Bhabhas $N_{tot} = 2.7 \cdot 10^5$ per BX with $E_{tot} = 2.1 \cdot 10^3$GeV per BX (see figure 11 for production location of neutrons from different sources). The numbers of neutrons entering some individual detectors could be found in table 4 for the vertex detector, TPC and electro-magnetic calorimeter (barrel/endcap). The fluxes for the vertex detector are given as total fluxes for all neutrons and in brackets as fluxes normalized to 1MeV neutrons, weighted due to the silicon bulk damage by total non ionizing energy loss (NIEL).

In conclusion one can say that the fluxes at the vertex detector are in the order of $4 \cdot 10^8$ n/cm^2/year and that means both options (APS,CCD) seem to be possible in terms of the neutron background. The total numbers of neutrons of about 6000 per BX in the TPC and of about 4000 (8000) per BX in the ECAL barrel (endcap) seem to be a non critical amount of neutron background.

Table 4: Results from FLUKA98 for neutrons entering individual detector parts.

	VDET n (1MeV n) /cm^2/year	TPC n/BX (E_{tot}[GeV])	ECAL(b) n/BX (E_{tot}[GeV])	ECAL(ec) n/BX (E_{tot}[GeV])
n from BS	$2.8 \cdot 10^8$	2400	1800	2100
	$(0.5 \cdot 10^8)$	(5.1)	(4.3)	(3.7)
n from Pairs	$< 0.5 \cdot 10^8$	3200	2300	3100
	$(0.0 \cdot 10^8)$	(8.6)	(6.1)	(13.5)
n from RB	$< 0.5 \cdot 10^8$	44	31	2300
	$(0.0 \cdot 10^8)$	(0.002)	(0.001)	(13.5)
total	$< 3.8 \cdot 10^8$	5600	4100	7500
	$(0.5 \cdot 10^8)$	(13.7)	(10.4)	(30.7)

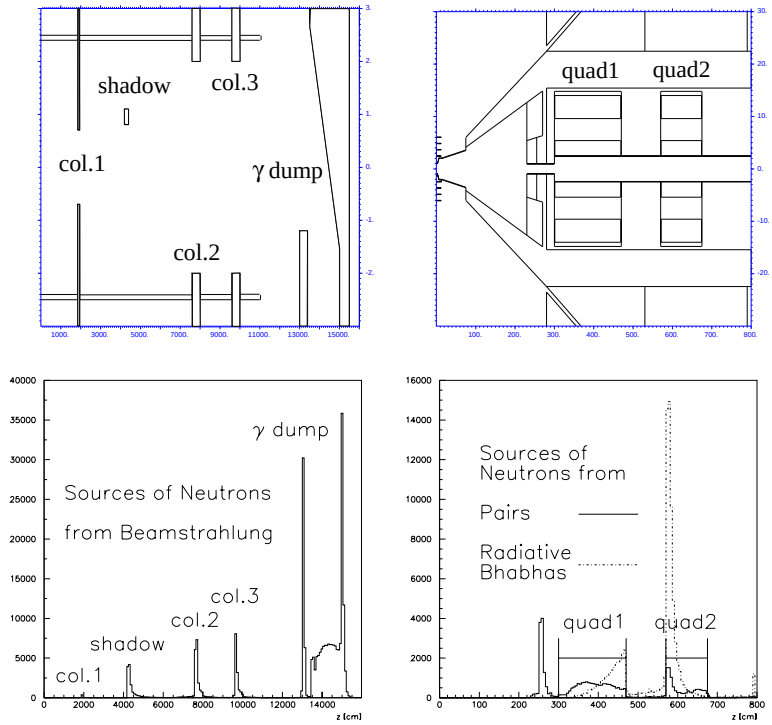

Figure 11: FLUKA98 geometry for TESLA beam line and mask region. Production location of neutrons for different sources: beamstrahlung, pairs and radiative Bhabhas.

4.6 Hadrons

An additional source of background is the production of hadrons by two colliding photons ($\gamma\gamma \to hadrons$). In this process the photons fluctuate into hadrons with the same quantum numbers and with a certain probability a photon can interact hadronically as a vector meson (mainly as ρ^0). Three cases are to be distinguished for the production of hadrons by two colliding photons:

direct once resolved double resolved

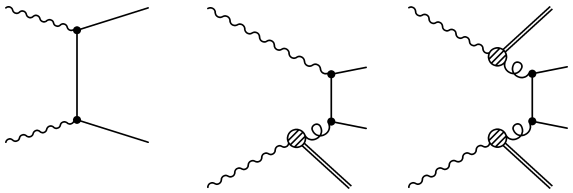

$\gamma\gamma \to jj$ $\gamma\gamma \to j_s jj$ $\gamma\gamma \to j_s j_s jj$

The simulation of $\gamma\gamma \to hadrons$ was done such as the photons were taken from the beamstrahlung simulation (GUINEA_PIG) and the $\gamma\gamma$ interaction was simulated by HERWIG 5.9, with multiparton interaction on and HERWIG default parameters except for the HERA DIS tuning [17]. In table 5 the results can be found for the three different cases. Only about $2 \cdot 10^{-2}$ events per BX are expected.

Table 5: Results for hadron production at TESLA.

type	events /BX [10^{-2}]	mult.	charg. mult.	E_{tot} /BX [GeV]
direct	0.53	15.2	8.5	0.25
single res.	0.40	30.5	15.7	0.32
double res.	1.12	44.7	22.2	1.50
all	2.05	34.3	17.4	2.07

From the TESLA detector simulation BRAHMS the following numbers for some detector parts were derived: In the first layer (2./3./4./5.) of the vertex detector 3.39 (0.66/0.42/0.29/0.23) $\cdot 10^{-3}$ charged hits per cm^2 per BX were found for a main magnetic field of 3T. In the TPC 8.5 gammas per BX with a mean energy of 2.6MeV and 0.7 charged particles per BX were found. The energy flow into the ECAL barrel is 2.0GeV per BX and 4.0GeV per BX for the endcap. In conclusion one can say that the hadron background found in the detector is small.

4.7 Muons

In e^+e^- linear colliders muons are produced in electro-magnetic beam-nucleon interactions in the beam delivery system due to partial beam loss in beam line elements. They can contribute an intolerable background in the detector. When electrons or positrons strike beam line elements muons are produced by a variety of mechanisms: Bethe-Heitler process ($\gamma Z \to \mu^+\mu^- Z$, dominant), photo production of π ($\gamma Z \to \pi(\to \mu\nu) + X$) and direct annihilation ($e^+e^- \to \mu^+\mu^-$). Even the muons produced far away from the IP can traverse the tunnel parallel to the beam line and reach the detector. Therefore in the simulation all beam line elements of the beam delivery system (-1200m $\to$ IP) and the tunnel are included. The dominant channel $\gamma Z \to \mu^+\mu^- Z$ was investigated in the current simulation studies. The detector is defined as a disk of radius 4.5m at the IP. A detailed description of this study can be found elsewhere [18]. The results of this simulation can be seen in figure 12, where the number of lost electrons to produce one muon in the detector is plotted as a function of the source location.

One finds in average about $2.5 \cdot 10^4$ lost electrons to get one muon in the detector. Additional magnetized iron toroids (2 toroids a 9m at 866m/1060m from the IP) help to reduce the muon background by a factor 10. Introducing an iron doughnut (120m iron at 800m) helps to reduce the muon background by a factor of 1000.

4.8 Backscattered Synchrotron Radiation

Synchrotron radiation will be produced by the incoming beam in the magnetic field of the last bending magnet. Also in the field of the final quadrupole doublet synchrotron radiation will be produced by the incoming and outgoing beam. The collimation system is made such that no direct synchrotron radiation hits any part of the detector, but backscattered photons can be a potential background source for

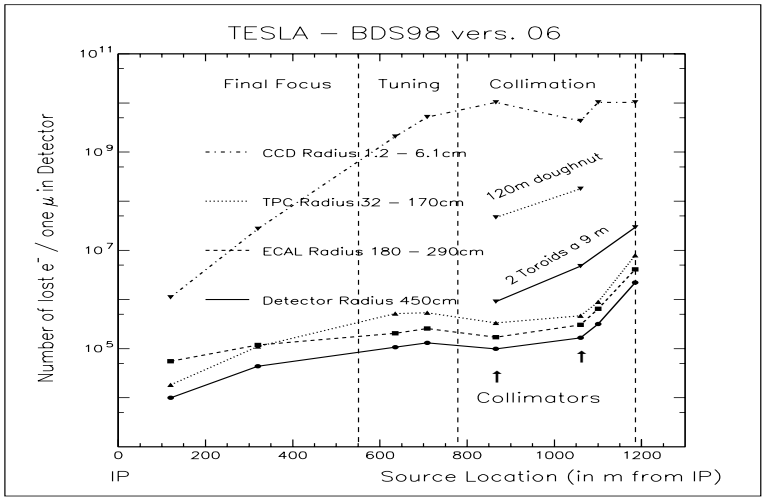

Figure 12: Number of lost electrons needed to produce one muon in the detector as a function of the source location.

the detector. The main source for backscattered synchrotron radiation is the first collimator at 19m from the IP. Table 6 shows the amount of synchrotron radiation hitting the first collimator. The calculation of backscattered synchrotron radiation into the detector takes into account the energy spectrum, the angular distribution and the albedo of the collimator material, resulting in 60 photons per cm^2 per BX in the vertex detector with energies of E_γ <1MeV. Approximately no backscattered photons reach the TPC and the ECAL.

Table 6: Synchrotron radiation hitting the first collimator.

source	N_γ	scattering	N_γ (scat. at col.1)
inc. beam/last bend	$5 \cdot 10^{10}$	edge + back	10^8/BX
inc. beam/final quad	$2 \cdot 10^{11}$	back	10^8/BX
out. beam/final quad	$4 \cdot 10^{11}$	back	$2 \cdot 10^{11}$/BX

4.9 Beam-Gas

The main sources of rest gas inside the beam pipe are on the one hand the material outgasing, which is a global effect and on the other hand the synchrotron radiation, which is a local effect. For the simulation of the beam-gas interaction it was assumed to have as rest gas CO with a pressure of $p = 5 \cdot 10^{-9}$mbar. Tracking was performed through the last 600m of the beam line, including quadrupoles, collimators, mask and a beam pipe of 1cm radius.

As result there were $3 \cdot 10^{-3}$ electrons per bunch crossing found which are leaving the beam pipe near the IP with an energy of about $E \approx 0.2 \cdot E_{beam}$. So the background expected in the detector from beam-gas interactions will be very small.

Table 7: Summary of all background sources at TESLA for beamstrahlung (BS), pairs (PA), radiative Bhabhas (RB), neutrons (N), hadrons (HA), muons (MU), backscattered synchrotron radiation (BSR) and beam-gas interaction (BGI).

Source	N_{tot} /BX	E_{tot} GeV/BX	VDET hits/cm^2/BX	TPC /BX	EC(b) /BX	EC(ec) /BX
BS	$6.6 \cdot 10^{10}$	$2.8 \cdot 10^{11}$	-	-	-	-
PA	$1.2 \cdot 10^{5}$	$3.0 \cdot 10^{5}$	690 (1.layer, 3T)	1350γ (3T)	-	-
RB	$4.9 \cdot 10^{4}$	$2.6 \cdot 10^{6}$	2 (1.layer, 3T)	3γ (3T)	-	-
N/BS	$2.5 \cdot 10^{10}$	$2.4 \cdot 10^{8}$	$2.8 \cdot 10^{8}$ n/cm^2/year	2400	1800	2100
N/PA	$4.9 \cdot 10^{4}$	262	$< 0.5 \cdot 10^{8}$ n/cm^2/year	3200	2300	3100
N/RB	$2.7 \cdot 10^{5}$	$2.1 \cdot 10^{3}$	$< 0.5 \cdot 10^{8}$ n/cm^2/year	44	31	2300
HA	$2.1 \cdot 10^{-2}$ events	2.1	$3.4 \cdot 10^{-3}$ (1.layer, 3T)	8.5γ (3T) 0.7char.(3T)	2.0GeV	4.0GeV
MU	$2.5 \cdot 10^{4}$ N_e/μ		$2.5 \cdot 10^{7}$ N_e/μ	$1 \cdot 10^{5}$ N_e/μ	$5 \cdot 10^{4}$ N_e/μ	$5 \cdot 10^{4}$ N_e/μ
BSR	$2.0 \cdot 10^{11}$	$2.0 \cdot 10^{8}$	60γ/cm^2/BX	-	-	-
BGI	$3 \cdot 10^{-3}$	0.15	-	-	-	-

5 Conclusion

The IR picture described in this paper offers a coherent solution to the beam transport and detector protection assuming the most demanding beam and detector conditions considered up to now for TESLA, namely:

- High luminosity $L = 3 \cdot 10^{34}\text{cm}^{-2}\text{s}^{-1}$, corresponding to the beam parameters with high beam-beam disruption
- Capture and transport of the e^- spent beam after collision, towards the positron source target
- Vertex detector of about 1cm radius, combined with high solenoid field of 4T

While the global design of the collider design is under progress, these options are still being discussed. If some of them are eventually removed, we believe that the IR design can only be easier and its layout simpler. The 800GeV center of mass energy option of TESLA has also been studied and does not change qualitatively the conclusions reached in this study. Vertical stabilization of the beam collision by a bunch-to-bunch feedback system is necessary and feasible. Limiting the maximum luminosity loss due to bunch separations to less than 10% relaxes the rms tolerance of the final doublet pulse-to-pulse displacements to 200nm.

The comparison of the generation of beamstrahlung and pairs between three different simulation programs showed reasonable agreement. From the background from pairs and radiative Bhabhas found in the detector one can conclude that the instrumentation of the mask will be possible down to 23.5mrad and that for the vertex detector both pixel options (APS,CCD) are possible. The neutron flux in the vertex detector was found to be moderate, so that also from this side both options (APS,CCD) seem to be feasible. The neutron background in the TPC and the ECAL seem to be handleable. Only small amounts of background signals from hadrons, backscattered synchrotron radiation and beam-gas interaction were found

in the detector (see table 7). So we can state that with the present knowledge of background at TESLA we foresee no problems for the presently studied detector design.

Acknowledgments

We are particularly grateful to D. Schulte and A. Drozhdin for their valuable help and advice while this study was being done. We also would like to thank R. Brinkmann, R.-D. Kohaupt, S. Schreiber and N. Walker for many useful discussions. Finally we thank A. Ferrari for providing us with the program FLUKA98.

References

1. R. Brinkmann, G. Materlik, J. Rossbach, A. Wagner, *Conceptual Design of a 500 GeV e^+e^- Linear Collider with integrated X-ray Laser Facility*, DESY 1997-048, 1997; ECFA 1997-182, 1997
2. R. Brinkmann, *High Luminosity with TESLA 500*, DESY, TESLA 97-13, 1997
3. J.M. Rifflet et al., *Cryogenic and Mechanical Measurements of the first two LHC lattice Quadrupole Prototypes*, EPAC94 Conf., London, UK, 1994
4. D. Schulte, *Study of Electromagnetic and Hadronic Background in the Interaction Region of the TESLA Collider*, Ph.D. Theses 1997, DESY TESLA 97-08, 1997
5. D. Schulte, *Beam-Beam Simulation with GUINEA_PIG*, ICAP Conf., Monterey, CA., U.S.A., 1998; CERN/PS 99-014, 1999
6. A. Devred, private communication
7. O. Napoly, D. Schulte, *Luminosity Monitor Options for TESLA*, LINAC98 Conf., Chicago, U.S.A., 1998
8. N. Walker, private communication, DESY 1999
9. I. Reyzl, *Fast Feedback Systems for Orbit correction in the TESLA Linear Collider*, IEEE Conf. Proc. of the PAC 99, New York, U.S.A., 1999
10. J. Rümmler, *Feedback Kickers in the DESY Rings*, IEEE Conf. Proc. of the EPAC 94, London, England, 1994
11. P. Bambade, R. Erickson, *Beam-Beam Deflection as an Interaction Point Diagnostic for the SLC*, SLAC-PUB 3979, 1986
12. K. Yokoya, T. Tauchi et al., *Program CAIN 2.1b*, http://www-acc-theory.kek.jp/members/cain
13. V. Telnov, *Program LINCOL 1.0*, private communication
14. *GEANT, Detector Description and Simulation Tool*, CERN Geneva, Switzerland 1993
15. T. Behnke, G. Blair et al., *BRAHMS - Version 1.02, A Monte Carlo for a Detector at a 500/800 GeV Linear Collider*, http://www.ifh.de/linear_collider
16. A. Fasso, A. Ferrari, J. Ranft, P. Sala et al., *Program FLUKA98*, manual and code available from authors
17. N. Brook et al., *Tuning Monte Carlo Event Generators to HERA Data*, UCL/HEP 96-05, 1996
18. M. Sachwitz, H.J. Schreiber, *Muon Background in a 500GeV TESLA Linear Collider*, DESY, TESLA 94-27, 1994